Charge Trapping in Bright and Dark States of Coupled PbS Quantum Dot Films

Jianbo Gao and Justin C. Johnson*

National Renewable Energy Laboratory, 1617 Cole Boulevard, Golden, Colorado 80401, United States

ABSTRACT

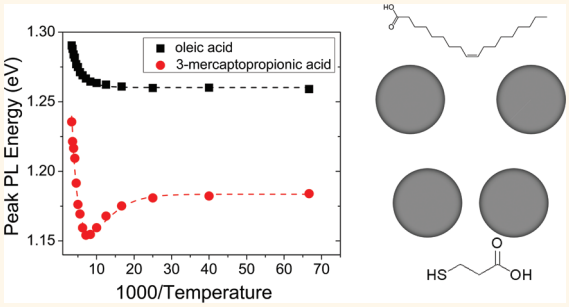

Analysis of photoluminescence (PL) from chemically treated lead sulfide (PbS) quantum dot (QD) films versus temperature reveals the effects of QD size and ligand binding on the motion of carriers between bright and dark trap states. For strongly coupled QDs, the PL exhibits temperature-dependent quenching and shifting consistent with charges residing in a shallow exponential tail of quasi-localized states below the band gap. The depth of the tail varies from 15 to 40 meV, similar to or smaller than exponential band tail widths measured for polycrystalline Si. The trap state distribution can be manipulated with QD size and surface treatment, and its characterization should provide a clearer picture of charge separation and percolation in disordered QD films than what currently exists.

KEYWORDS: nanocrystal · photoluminescence · transport · exciton · band tail · temperature

Lead chalcogenide quantum dots (QDs) have shown great promise as active components in photovoltaic (PV) cells. Power conversion efficiencies of solar cells using thin, densely packed layers of PbS QDs for light absorption have risen from 2% just a few years ago[1] to approaching 6% today.[2,3] In addition to the potential for high efficiency, strong quantum confinement and the possibility of multiple exciton generation (MEG)[4] make these materials scientifically interesting counterparts to conventional bulk semiconductors used in PV. The observation of extremely high one sun photocurrent (>25 mA/cm^2) is particularly intriguing,[5] considering the expected difficulty in transporting charges quickly and efficiently through a highly disordered and surface-dominated nanocrystalline system. Different models have been invoked to explain transport phenomena in QD films, ranging from tunneling[6] and hopping[7,8] to coherent "band-like" transport.[9]

Most transport models for QDs have considered charges residing in quantum-confined core exciton states inhibited from free motion by potential barriers due to the dielectric surrounding, site energy disorder, and Coulomb charging. However, little attention has been paid to the possible role of sub band gap states in transport despite evidence that such states are present even in the absence of surface oxidation. A recent investigation by Nagpal and Klimov[10] discovered deeply trapped carriers in a small size range of treated PbS QDs using optical field effect transistor measurements, and others have concluded similarly.[11] Recent studies have also rejected the notion that site energy disorder or Coulomb charging alone inhibit the charge transport at room temperature,[12] which leaves the conclusion that trap or surface states likely contribute significantly under realistic conditions (i.e., zero or low bias and room temperature).

Electronic structure calculations on PbSe and PbS QDs initially rejected the notion of any sub band gap states.[13,14] However, the known nonstoichiometry of the PbSe and PbS surfaces[15] and the chemical changes that occur upon ligand exchange[16] have led to reconsideration of whether states within the gap related to surface termination can be considered irrelevant. Several recent investigations have found evidence for sub band gap states in isolated PbS or PbSe QDs by photoluminescence (PL).[17−19] The exact nature of these states remains elusive, although our recent investigations suggest it may be related to the nonstoichiometric surface (i.e., Pb dangling bonds). While surface trap states can almost certainly be manipulated through choice of ligand and capping shell chemistry, few detailed studies have been performed to demonstrate this conclusively. Chemical treatments typically

* Address correspondence to justin.johnson@nrel.gov.

Received for review January 16, 2012 and accepted March 23, 2012.

Published online March 30, 2012
10.1021/nn300707d

remove the native oleate cap and replace it with shorter ligands, which necessarily bring the QDs into close proximity and cause energy or charge transfer and a red-shifted absorption due to both dielectric and wave function delocalization effects. These complications often make it difficult to extract effects solely due to surface chemistry. Coating the QDs with an inorganic shell may passivate some surface dangling bonds; however, without perfect lattice matching strain may induce new sub band gap states.[20] In addition, carriers can likely tunnel through a thin shell and be sensitive to the outer surface. Very thick shells can be grown,[21] but then at least one carrier type will be unable to tunnel and becomes immobile. It seems that in nearly all realistic QD photovoltaic device situations, trap states will be non-negligible.

Although PL is a commonly used tool for investigating QD photophysics, it less often used to assess transport. One reason may be the misconception that emission should be entirely quenched in electronically coupled films. Although PL is often strongly quenched by fast charge separation in coupled QDs at room temperature, emission is more likely at lower temperatures. The spectral shape and quenching behavior of PL vs. temperature can thus serve as a probe of the localized state distribution. Moreover, if charges in trap states can recombine radiatively, the low temperature PL observed under steady state conditions arises from the lowest energy states in the distribution, which are energy "sinks" that can dictate the device efficiency. It is important to note that although local charge separation may quench PL significantly there may not be a direct relationship to electrical measurements of transport that rely on long-range movement of carriers to electrodes. In that sense, PL measurements may be more akin to spectroscopic probes of short-range mobility such as time-resolved terahertz or microwave conductivity that also probe carrier motion in a "contactless" manner.[22,23] With this in mind, one must use caution when directly comparing PL results with electrical measurements on thick films involving charge transport to contacts.

Whereas in isolated QDs surface states are probably entirely localized, the network of tightly coupled crystals in treated QD films may resemble that of bulk-like polycrystalline or amorphous semiconductors, in which true delocalization is prevented by disorder. An exponential band tail model is commonly invoked in such situations, and it is thought to arise from lattice termination effects at interfaces and/or potential fluctuations due to charges trapped at surface dangling bonds. Some past PL studies, particularly on polycrystalline and amorphous Si, have attempted to make a connection between emission spectra and band tail states.[24,25] Charge transport can occur by multiple trapping, in which the depth of the tail, manipulated using material quality and surface passivation,[26] is a crucial parameter. Evidence for exponential band tails has also been observed in absorption measurements,[27,28] but it may be particularly difficult to identify narrow band tails in QD films due to the large size distribution and the small absorption coefficients for transitions to localized band tail states. Although in these disordered systems PL primarily arises from sub band gap states, even in fully optimized PV devices with such states removed reasonably strong PL should be observed due to thermodynamically mandated radiative recombination.[29,30]

Herein we investigate PL from PbS QDs of various sizes vs. temperature and chemical treatments. We find a critical PL quenching temperature for each size and surface treatment that corresponds to the thermal energy needed for promotion of charges from sub band states to higher mobility states that engender fast charge motion and eventual retrapping in dark states. We discuss the variation of the quenching temperature and PL peak through the sample set with respect to possible sources of an activation barrier. We find a particularly close correspondence with PL data attributed to band tail states in polycrystalline and amorphous Si, suggesting that a similar "tail" of states may exist in the transport gap of coupled QD films. This "tail" is an emergent property in films that may not be readily predicted by optical studies of isolated QDs but is essential to understand because of its strong influence on transport.

RESULTS

Absorption spectra of PbS QD samples capped with oleic acid (OA) in tetrachloroethylene solution are shown in Figure 1A. The size distributions range from 140 to 250 meV (full width at half-maximum) for the different samples as judged by the lowest exciton absorption width.[31] Absorption spectra for films treated with various chemicals are shown in Figure 1B. These treatments are known to quantitatively remove the OA cap and replace it with the shorter ligand.[32] Note that although there is a clear red shift in all treated films, the exact position of the peak is obscured by scattering and interference effects. In Figure 2, PL spectra for QDs cast into films are displayed for two sizes: 2.6 nm diameter (810 nm first exciton peak) and 3.9 nm diameter (1100 nm first exciton peak). For the treated films, the largest red shift and greatest broadening occur for the shortest ligand, formic acid (FA), while the smallest red shift occurs for the longest ligand, 3-mercaptopropionic acid (MPA). Overall PL intensity is also shown to decrease with shorter ligand length, with the largest decrease occurring between OA and MPA. An accurate PL quantum yield Φ_{PL} could not be determined at 13 K, thus the relative intensities shown in Figure 2 contain some uncertainty due to varying film properties such as thickness and roughness. However, films were fabricated to absorb at least

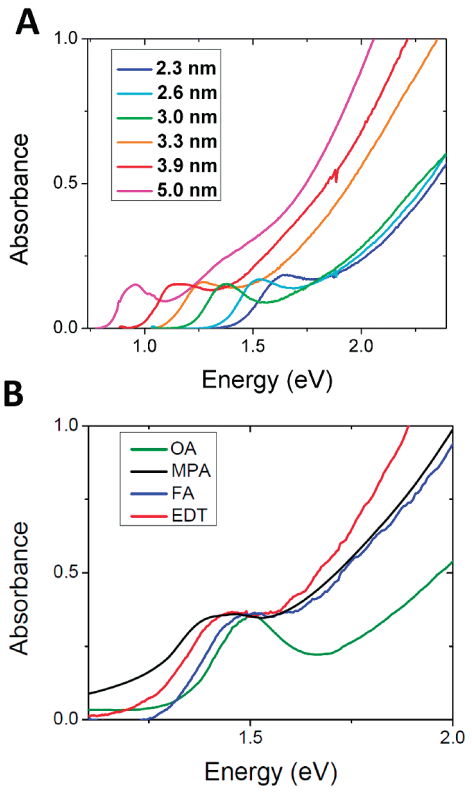

Figure 1. (A) Absorption spectra for PbS QD samples in TCE solution. (B) Absorption spectra for 2.6 nm QD films and four chemical treatments.

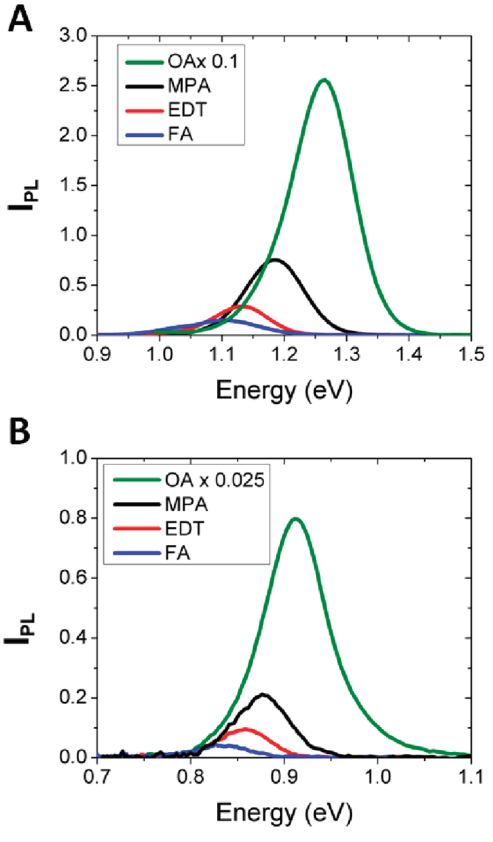

Figure 2. Emission spectra of (A) 2.6 nm and (B) 3.9 nm PbS QD films at 13 K with various chemical treatments.

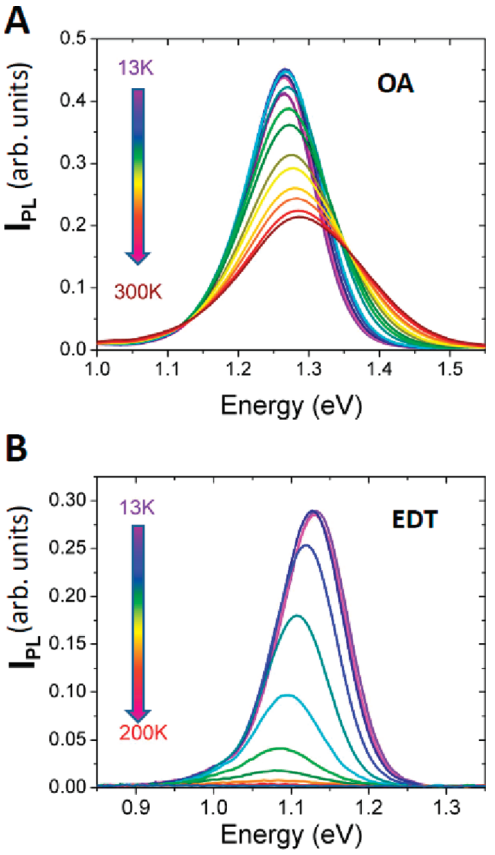

Figure 3. Emission spectra vs temperature for (A) untreated and (B) EDT treated 2.6 nm QD films.

90% of all incoming laser light at 488 nm, and PL collection efficiency uncertainty is not expected to cause variations of more than about 20%. Figure 3 shows a representative spectral series vs. temperature for $d = 2.6$ nm QDs with and without 1,2-ethanedithiol (EDT) treatment. Much stronger thermally activated quenching is seen in the case of all treated films vs. untreated films, suggesting relatively facile separation of charge carriers as temperature increases due to inter-QD coupling. In addition, the PL peak shifts to lower energy by as much as 25 meV with increasing temperature for the EDT treated film, opposite to the behavior of uncoupled films. The known band gap shift increases the exciton absorption energy on the order of 0.01−0.15 meV/K for the sizes of QDs studied here,[33] thus the red shift in PL is not simply due to band gap shifting. Treated and untreated films show similar band gap shifts with temperature (Figure S3C, Supporting Information), although the considerable width and optical interference from treated films makes accurate determination of shifts <0.03 meV/K difficult.

Figure 4 shows the integrated PL intensity vs. inverse temperature for two sizes and all treatments of QD films. The nature of the functional group of the ligand affects how much thermal energy, identified as T_Q, is needed to quench the emission. The values of T_Q for different treatments and QD sizes are shown in

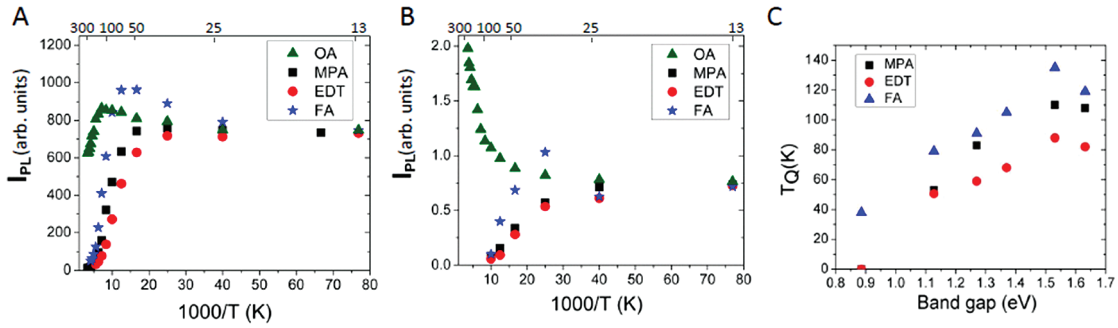

Figure 4. Emission quenching curves for various treatments of (A) 2.6 nm and (B) 3.9 nm PbS QDs. (C) T_Q values extracted from fits of $I_{PL}(T)$ with eq 1 vs QD band gap.

Figure 4C. T_Q is determined from fitting normalized integrated PL vs. T to a Boltzmann model of thermal quenching:

$$I_{PL}(T) = 1/(1 + \exp[((T - T_Q)/\phi]) \quad (1)$$

with T_Q and ϕ as the fitting parameters. Despite FA having the shortest length (and the strongest red shift in low T PL), T_Q is highest for films treated with FA. This is unexpected from an interdot spacing perspective, since barriers to charge separation should be lower with a smaller region of dielectric between QDs. There is also a clear size dependence of T_Q, increasing for smaller sizes of QDs. While the 13 K emission from treated films maintains a fairly constant integrated intensity for sizes <4 nm, the PL is reduced by at least 1 order of magnitude for QDs of $d = 5$ nm and $d = 7$ nm. Of these larger QD samples, only FA-treated 5 nm PbS QDs were analyzable with eq 1, while other films exhibited weak and nearly temperature-independent emission.

Figure 5A displays the temperature dependent shift of the PL peak, defined as E_{pk} and determined from fitting the spectrum with a single Gaussian. The typical PL peak shift for an untreated film (partially due to band gap shift and partially to population redistribution between band and sub-band levels), represented by the OA capped QD film (black squares), causes E_{pk} to shift to the blue with increasing temperature.[17] Anomalous PL shifting is observed for all treated films, with the peak shifting to the red from 13 K to about 80−140 K before shifting back at higher temperatures. The temperature at which E_{pk} is minimized, T_{min}, is size and treatment dependent, decreasing with increasing size. Values of T_{min} for all sizes and treatments are collected in Table 1. The dashed lines in Figure 5 are representations of a single (black, eq 2a) and double (red, eq 2b) oscillator Bose-Einstein model:

$$E_{pk}(T) = E_0 + a\theta/(\exp[\theta/k_BT] - 1) \quad (2a)$$

$$E_{pk}(T) = E_0 + a_1\theta_1/(\exp[\theta_1/k_BT] - 1) - a_2\theta_2/(\exp[\theta_2/k_BT] - 1) \quad (2b)$$

Equation 2a can be used to describe band gap shifting vs. temperature through phonon occupation statistical

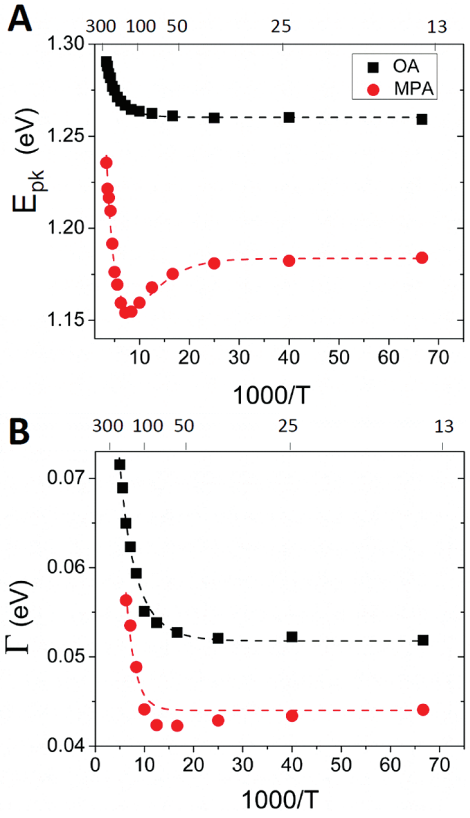

Figure 5. (A) E_{pk} and (B) Γ vs temperature. Dashed lines are fits discussed in the text.

factors.[34,35] The additional term in eq 2b is used to account for the red shift of the PL band for coupled QDs. The width, Γ, of the PL peak in treated films also reaches a minimum that occurs at slightly lower temperature than the minimum in PL peak energy (Figure 5B). All samples show a sharp increase in both Γ and E_{pk} as T approaches room temperature, but only the strongly coupled QD samples show a minimum in both Γ and E_{pk}. The peak narrowing occurs despite the usual phonon-mediated broadening mechanisms that cause a monotonically increasing line width in untreated samples (Figure 5B, black squares). This thermally activated broadening is also fitted with a single oscillator Bose-Einstein population model

TABLE 1. T_Q, T_{min}, and $1/\beta$ for Various Sizes and Treatments[a]

	2.3 FA	2.3 EDT	2.3 MPA	2.6 FA	2.6 EDT	2.6 MPA	3.0 FA	3.0 EDT	3.0 PDT	3.0 BDT	3.3 FA	3.3 EDT	3.3 MPA	3.9 FA	3.9 EDT	3.9 MPA
T_Q	119	82	108	135	88	110	105	68	80	132	119	59	83	79	51	53
T_{min}	160	160	140	180	120	130	160	100	120	140	120	100	100	80	80	70
$1/\beta$	32	23	29	42	24	27	25	19	21	38	24	17	21	20	15	17

[a]Diameter in nm and chemical treatement is shown for each sample. Temperature values are in K while $1/\beta$ values are in meV. β was derived from simulations described below. Clear PL quenching behavior was not observed for 5.0 or 7.0 nm QDs.

(dashed lines, eq 2a), which describes the temperature-dependent distribution of phonons. A good fit is obtained for untreated QDs, but a clear discrepancy between model and data is found for the treated film near the position of the minimum in Γ. The depth of the minimum in Γ appears to be sample dependent, which probably indicates variations in peak broadening mechanisms (homogeneous and heterogeneous).

Increasing the excitation power does not strongly affect the shape of PL spectra for treated films but causes a 9 meV blue shift in the emission peak. For untreated films the shift in the emission peak is much smaller (4 meV) (Figure S2, Supporting Information, 3.3 nm QDs). The shift of the PL peak in untreated films may be attributed to slight sample heating causing the band gap to increase at higher powers, while in treated films a factor in addition to heating must cause the larger blue shift. The intensity dependence of integrated PL depends on temperature for treated films, following a power law $I_{PL} = P^x$ of about $x = 1.0$ at higher temperatures (>70 K) while decreasing to $x = 0.65$ at 13 K (Figure S1C, Supporting Information). A significant increase in lifetime of the carriers at low temperatures (e.g., by freezing into "dark" exciton states) could be invoked to explain the sublinear power dependence. The PL lifetime has been shown to increase at low T in untreated PbS and PbSe QDs,[34,36] which may be indicative of a redistribution of population from bright to dark exciton states but may also represent changing nonradiative decay rates. In a study that observed the bright-dark exciton transition in PbSe QDs using magnetic field effects, the extent of the lengthening of the radiative lifetime (~50%) and the temperature at which it occurs (<1 K) are not consistent with the onset of saturation observed here.[37] Therefore, the saturation and the peak blue shifting more likely represent redistribution of population within the manifold of bright states as opposed to population flow among bright and dark. Unlike treated films, increasing power on untreated films causes a change in spectral shape (Figure S2, Supporting Information), implying that more than one emitting species is present and that increased power alters the population distribution between these two states by saturation of the lower energy component.[17]

We have also compared PL spectra vs. T for QD films treated with ligands of differing length but the same terminating functional groups. EDT, 1,3-propanedithiol (PDT), and 1,4-butanedithiol (BDT) were used to treat 3.0 nm (900 nm first exciton) QD films. Thermal quenching of the PL (Figure 6A) and shifting of the PL peak (Figure 6B) are observed for the treated films. Data for OA capped QDs are shown for reference. T_Q increases with increasing chain length while the red shift of E_{pk} decreases as the chain lengthens. Furthermore, the minimum in the PL peak position occurs at higher temperature for longer ligands, becoming very shallow by BDT. Trends for PDT are more similar to those of EDT than of BDT despite the equal addition of just one C–C bond through the series.

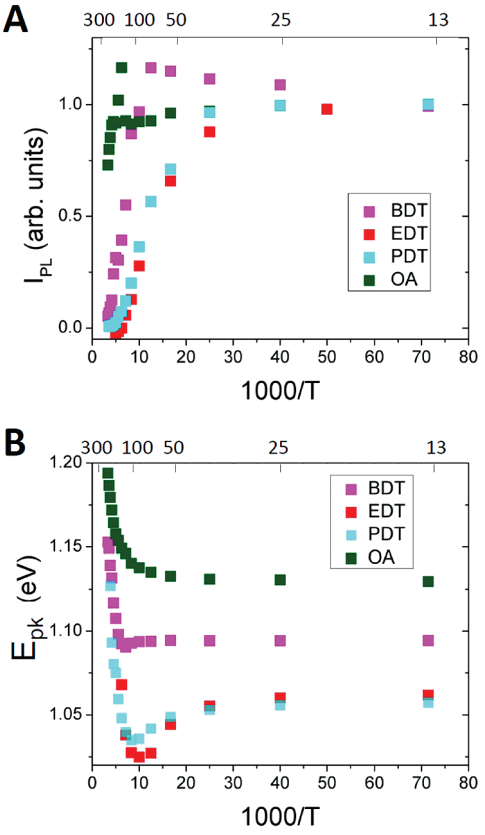

Figure 6. (A) Quenching of integrated PL and (B) shift of PL peak vs temperature for 3.0 nm PbS QD films treated with three dithiol chains compared with OA.

DISCUSSION

Origin of PL in Coupled QD Films. The modest red shift and the persistence of an excitonic feature in absorption for treated films suggest that quantum-confined excitons are initially formed upon photoexcitation

(Figure 1). The observation of an excitonic peak of even highly coupled films[38] likely results from the retention of a localized ground state that has its largest transition moment coupling to a quantum-confined exciton state. If coupling between QDs is large, subsequent exciton delocalization and/or fast charge separation occurs.[9] In highly coupled and disordered systems, geminate recombination is typically not competitive with fast charge separation while deep trapping and nonradiative decay dominate nongeminate radiative recombination. The identity of dark traps cannot naturally be determined from PL studies, but they may be related to the "mid-gap band" discussed in ref 10. Since even in untreated PbS QDs the PL quantum yield falls well below 100%, it is likely that dark traps are present intrinsically and do not arise from treating with short chain ligands.[39]

Our previous measurements of PL on untreated PbSe QDs led us to assign the emission at low temperature to shallow "trap-to-band" carrier recombination, in which carriers quickly trap in states below the lowest quantum-confined core exciton level.[16,17] This assignment was based upon: (i) the known nonstoichiometry of lead chalcogenide QDs, in which imperfect passivation of higher energy surfaces induces electron trapping;[15] (ii) manipulation of the temperature-dependent emission with size and surface treatment;[16] (iii) experimental evidence for a size-independent bright sub-band gap energy level in PbS;[18,19] and (iv) reference to similar material systems in which trap states have been observed.[40,41] A clear distinction between "trap-to-band" and dark exciton emission in isolated QDs may be difficult to detect spectroscopically, especially if the exciton is not truly "dark" (i.e., its radiative rate is not much different from that of the bright exciton) or if the dark-bright splitting is large and strongly size-dependent. Classic evidence for trap vs. band states that usually arises from widely separated spectral features, vast lifetime differences, or power dependence variations are all lacking in this unique material system. The difference between these models may not be best judged by measurements of exciton and carrier dynamics in isolated QDs but rather in coupled QD arrays, where the properties of the excited states may become more evident.

Thermally activated PL quenching and shifting could result from several effects: (i) exciton migration following population flow from dark to bright exciton states, (ii) exciton binding energy, (iii) site energy disorder of QD samples, (iv) Coulomb charging, and (v) interface or trap states.

(i) Dark exciton states, known to exist in CdSe[42] and predicted in PbS/PbSe,[43] are split from bright exciton states by a few to a few tens of meV and have a smaller radiative rate than bright states. The disagreement between experimental measurements of the dark-bright splitting (<0.3−0.9 meV[37]) and calculations (2−17 meV[43]) for sizes similar to those studied here leaves some uncertainty about the temperature range for which population flow should occur. Exciton migration by dipole−dipole interactions among dark states should be exceedingly slow and not strongly temperature dependent. However, thermal promotion of excitons from dark to bright states has been proposed to "activate" energy transfer in uncoupled QD films,[44,45] and this could cause a red-shift of emission if the radiative rates and energy transfer times are balanced. This balance should be delicate and easily altered both by the size dependence of the dark-bright exciton splitting and the interparticle spacing R that affects the energy transfer rate as $1/R^6$. In addition, the strong quenching of PL at all temperatures for coupled films with QDs above a certain size is difficult to explain with this model. Other work on radiative lifetimes vs. QD size and coupling strength has also suggested such energy transfer is not the cause of strong PL quenching.[46]

(ii) From a simple electrostatic perspective, separation of the charges from a $1S_e-1S_h$ exciton would require thermal energy in excess of the exciton binding energy. When additional potential barriers to charge separation are reduced by bringing the QDs into close proximity, the exciton binding energy alone could provide a barrier to charge separation.[46] The exciton binding energy decreases with increasing size, predicting a lower temperature of PL quenching as QDs gets larger. However, the exciton binding energy is not expected to fall below 1 meV for intermediate size QDs (5 nm),[47] which conflicts with our observation of nearly full PL quenching for this size at low T. In addition, any PL shifting would likely be toward higher energies as *T* increases because lower band gap QDs would ionize first, opposite to what is observed.

(iii) If carriers must access the $1S_e$ ($1S_h$) QD levels for efficient transport, site energy disorder $\Delta\alpha$ (i.e., size heterogeneity) would produce a tortuous energy landscape because of the variation of the energy of these levels with size. Samples measured here would require significant heating (>1000 K) for carriers to be thermally distributed throughout the $1S_e$ ($1S_h$) levels of the ensemble. However, since PL quenching only requires local charge separation, thermal energies of a few to a few tens of meV (10−325 K) might promote charge motion in lower energy QD subensembles. It has also been suggested that these low energy subensembles may dictate transport by forming a percolation network through the tail of the $\Delta\alpha$ distribution.[12] PL would be quenched and red-shifted as temperature increases, consistent with observations. In addition, the actual magnitude of size heterogeneity would not be particularly important, since only the low energy tail of $\Delta\alpha$ is ever accessed during percolation. Intentional increases in $\Delta\alpha$ have also not severely limited carrier mobilities,[12] and thus it is clear that the magnitude $\Delta\alpha$

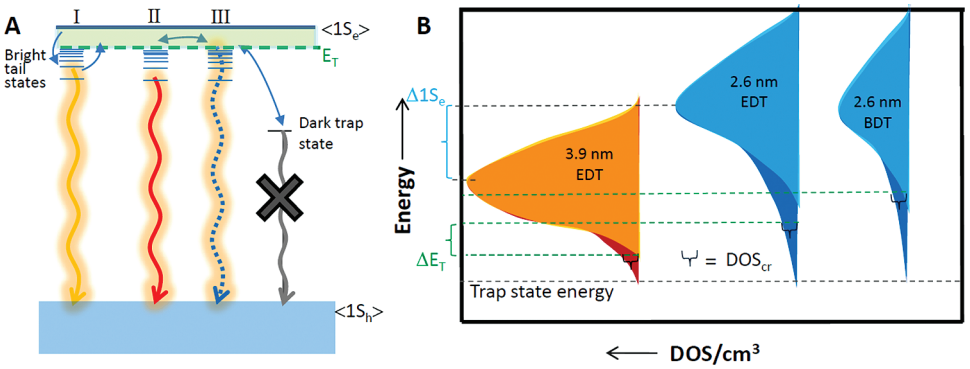

Figure 7. (A) Model of carrier dynamics vs temperature in a coupled QD film. I: Low temperature PL arises from carriers trapped in tail states. II: Intermediate temperature activates carriers in high energy tail states to the transport edge E_T, red-shifting the emission. III: Room temperature promotes most band tail carriers to the transport edge, where charge separation and multiple trapping leads to population of dark states and PL quenching. (B) Model of DOS vs energy for large (orange) and small (blue) QDs in coupled films. Darker feature underlying the lighter band is due to band tail states, which originate at the size-independent trap state level. Far right DOS profile has reduced overall DOS/cm^3 due to lower packing density with longer BDT ligand, which pushes E_T (and thus T_Q) higher. Average $1S_e$ level difference $\langle\Delta 1S_e\rangle$ and transport edge difference (ΔE_T) are shown along with the critical density of states (DOS_{cr}) necessary to achieve percolation. For large QD sizes, the $1S_e$ band falls below the trap state energy, eliminating the band tail.

by itself does not determine bulk transport. In addition, this model of thermally activated hopping between $1S_e$ ($1S_h$) levels in the tail of the distribution should not be strongly size-dependent, and a significant reduction in PL for films of coupled QDs with $d > 4$ nm is especially difficult to rationalize.

(iv) Another possible activation barrier to percolation may be the size dependence of the Coulomb charging energy, E_C. For a sample with no $\Delta\alpha$, E_C would be essentially zero, but E_C could vary by as much as a few meV if the entire ensemble is accessed during percolation, as charges move between QDs of differing sizes. Charging would add a small barrier to transport (and thus PL quenching), but it is likely to add little to the size dependence of the thermal activation.

Band Tail Model of PL Quenching. Although effects i–iv may have some influence on PL quenching, we find the overall picture somewhat unsatisfying, and present a model of the experimental observations invoking a prominent role for trap or interface states. Although in terms of densities of states the low energy tail of $\Delta\alpha$ may appear to be very similar to an exponential band tail, the physical origin is quite different. The exponential band tail assumes that delocalized band states are interrupted by disorder due to interfaces and/or potential fluctuations from trapped charges, whereas the exciton model, typically assumed for QDs, originates from core quantum confined states. In the limit of very strong inter-QD coupling, the models should merge. The justification for considering the exponential band tail model here is the use of "device-like" films of intimately coupled QDs with high charge carrier mobilities and composed of materials with high dielectric constants and low carrier effective masses. This set of properties should ultimately lead to very little distinction between steady-state behavior of colloidal QD films and conventional polycrystalline films.

The exponential band tail model has been shown to successfully describe PL behavior in bulk *poly*- or *a*-Si, causing a shifting of the peak PL energy with increased temperature due to preferential thermal depopulation of the higher energy side of the sub band gap distribution. We have adapted this model to QD arrays, as depicted in Figure 7. At low and intermediate temperatures, carriers very near the transport edge (E_T in Figure 7A) have enough thermal energy to be promoted and achieve significant mobility, and thus are unlikely to recombine radiatively, while carriers lying deeper in the band gap remain trapped. In Si strong red shifting of the PL was observed as the temperature was raised from 4 to about 50 K, above which the PL was strongly quenched.[48] Utilizing models developed for the exponential band tail of Si,[49] we have simulated PL spectra vs. temperature using eq 3:

$$I_{PL}(E,T) = Ae^{-\beta(E_{bg}-E)} \times (1-e^{-\beta(E_{bg}-E)})^N \times \left(1+\left(\frac{m}{e^{\frac{E_0-E}{kT}}-1}\right)\right)^{-1} \quad (3)$$

The model contains a line shape function (first two terms) and a term for thermal quenching, each of which is plotted in Figure 8A for typical parameter values. E_0 is the energy threshold for reaching the transport edge while E_{bg} is the band gap of the emitting species. N is related to the density of radiative tail states, m is the intrinsic detrapping rate divided by the radiative rate of the emitting state (set to 10^4, which would be 0.1 ns carrier release rate for a typical radiative lifetime of about 1 μs) and $1/\beta$ is the width of the exponential band tail. The line shape is approximately Gaussian, with a weak tail at lower energies. The peak narrows initially as temperature

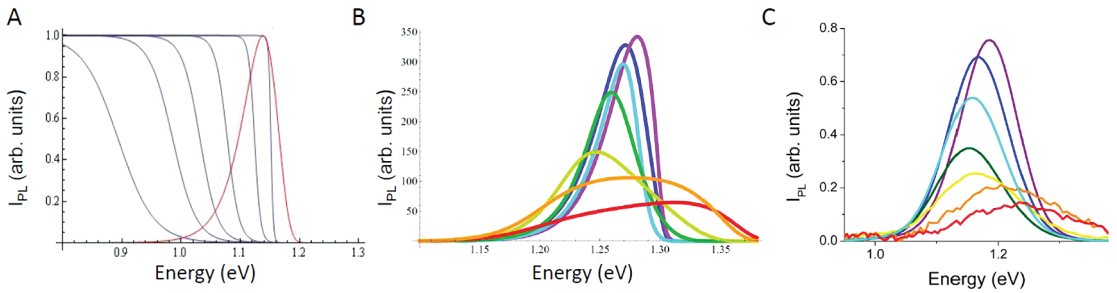

Figure 8. (A) Line shape (red) and quenching function (gray) arising from the first and second terms of eq 3, respectively. The blue curves are calculated from T = 10−300 K. (B) Simulated and (C) experimental spectra for 2.6 nm PbS QDs with MPA treatment. Simulation uses eq 3 and a linear shift of the band gap with temperature. PL amplitudes are scaled for clarity.

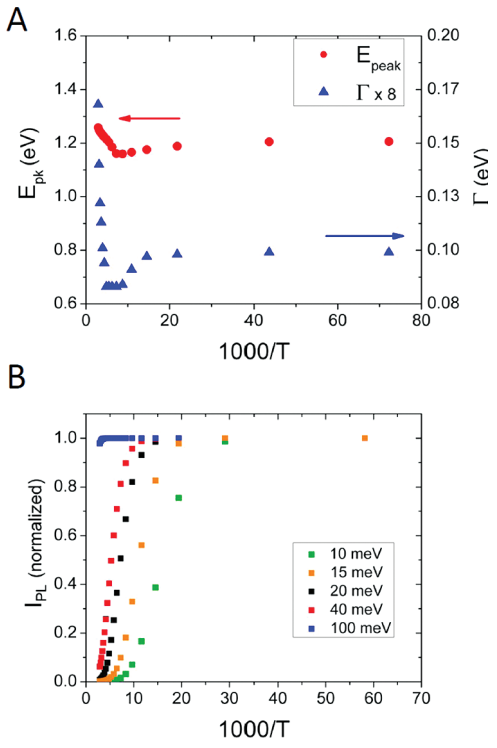

Figure 9. (A) Simulated $\Gamma(T)$ and $E_{pk}(T)$ for parameters to match 2.6 nm MPA treated PbS QDs. (B) Dependence of $I_{PL}(T)$ curves on $1/\beta$ for 2.6 nm QDs.

is increased due to the depopulation of the high energy side of the band. The peak then broadens significantly at high temperature as the quenching function flattens and amplifies the low energy tail. It is difficult to determine the exact PL line shape experimentally since the QD films are dominated by the inhomogeneous distribution of QD sizes. Nonetheless, the spectra are reasonably well-described by this function, especially when the full temperature range is examined. The spectrum broadens, red shifts, and becomes more symmetric as temperature increases (Figure 8B−C). The PL also quenches as temperature increases, and the predicted quenching curve shape and magnitude are similar to experimental data (Figure 9B).

Given the broadening and low PL signal at higher T, it was not possible to perform an accurate least-squares fit to the spectral series vs. T with eq 3. However, extracting E_{pk} and Γ from simulations using realistic values of the parameters produces temperature dependent trends that qualitatively match experiment (Figure 9A). The initial red shift in E_{pk} with T results from preferential depopulation of the high energy side of the band tail while the blue shift results from the flattening of the quenching function at higher T (Figure 8A) causing the distribution of emitting states to shift back toward its original position at low T. Of particular importance is the value of β, the band tail width. $1/\beta$ values as determined by reproduction of T_Q are found in Table 1. The theoretical dependence of T_Q on $1/\beta$ is demonstrated in Figure 9B, using integration of eq 3. Values for β were also determined by matching the minimum in E_{pk} with simulation, for which the same trend with size/treatment was found, but the values were found to be 20−40% lower than those found using T_Q for the same sample. Considering that all peak shifting mechanisms are not accounted for in the simulation, it is likely that β based upon T_Q matching is more accurate than that based on E_{pk}. There is some covariance between β and the difference between E_0 and E_{bg}. This covariance cannot be resolved here without further information about exactly what factors influence the Stokes shift. Spectral features for most samples are best reproduced for $E_0 \cong 0.95\ E_{bg}$, and to isolate the trend in β across the sample set E_0 was set equal to this value for data presented in Table 1. The fairly small band tail width predicted using the model represented by eq 3 may seem contradictory compared with the large Stokes shift (100−300 meV) for PL in these films at low T. Here, the Stokes shift is defined as the position of the PL peak with respect to the absorption peak. For an inhomogeneous sample the Stokes shift will be dominated by energy relaxation within the distribution that shifts the PL peak to much lower energy than its predicted zero-phonon position based upon the first exciton absorption. This Stokes shift is included in the simulations through the parameter E_{bg}, which is about 150−250 meV lower than the lowest exciton peak. $1/\beta$ is associated with the depth of the band tail below the transport edge, which must lie considerably below $\langle 1S_e \rangle$ due to the fast coupling-induced

relaxation within the QD ensemble. As shown in Table 1, for QD films the band tail depth can apparently be manipulated both by interfacial chemistry and by particle size.

Interestingly, because of the relatively small and positive shift of E_g vs. T for the size range of QDs studied here, thermal activation of carriers from the band tail produces a minimum of E_{pk} that is not observed in *poly*-Si or *a*-Si. The minimum in E_{pk} and the high temperature blue shift are still predicted to occur in the absence of any E_g shift but may be masked by the strongly negative E_g vs. T slope in many semiconductors, mitigating the shift in PL. Adding the expected temperature dependent band gap shift[33] of about 0.05 meV/K to eq 3 has little effect on the minimum in E_{pk} but does cause an increasing slope above 250 K (Figure 9A, red dots), in agreement with experiment. However, the considerable increase in E_{pk} toward room temperature cannot be captured by the absorption shift alone but instead requires an additional shift related to population flow between traps and core states.[17] The onset of the large slope in both E_{pk} and Γ vs. T occurs just above T_Q, suggesting that emission above this temperature is due to carriers near or above the transport edge that are either strongly coupled with phonons or have a large distribution of energies.

The trend of T_Q with QD size (Figure 4C), while noticeable, is only about 10 meV over the full size range, which is a small fraction of the change in confinement energy (~0.3 eV). If carriers were to require thermal activation from a localized, size independent trap state level to $\langle 1S_e \rangle$ for PL quenching, the expected T_Q trend with size should be much larger, up to about half of the change in band gap over the full size range (>0.1 eV).[40] The much weaker dependence observed suggests that the transport level does not rise in energy faithfully with $\langle 1S_e \rangle$ as size decreases. Instead, the density of band tail states increases and deepens as QD size decreases, counteracting the effect of a higher $\langle 1S_e \rangle$. The increase in band tail state density can be justified based upon the larger surface to volume ratio and the larger diversity of surface facets for smaller QDs. A representation of this effect is shown in Figure 7B, wherein the average $\langle 1S_e \rangle$ level changes much more drastically with QD size than does E_T. Although the weak dependence of E_T on size is still stronger than would be the case for transport through a high density of entirely isoenergetic trap states, it does relax the necessity for carriers to find proximate QDs within a narrow size range through which they must traverse, which would required if hopping were to occur only through core levels.

Another important observation is the loss of nearly all low temperature PL for QDs with $d > 5$ nm. The nearly complete quenching indicates either a crossing of energy levels or a changing surface chemistry with size. The crossing of a size-independent trap state level with that of the transport edge would reduce the equilibrium number of trapped charges and narrow the band tail, causing PL to be quenched even at low temperatures. This is represented by extrapolating the DOS profiles in Figure 7B to larger QD sizes with lower $1S_e$ energy, in which the tail of $\Delta\alpha$ crosses the trap state energy. The increased dominance of the {100} surfaces as PbS QD size increases is also expected to lower the concentration of electron surface traps,[16] which may reduce the depth of the band tail. One or both of these mechanisms may be responsible for enhanced PL quenching in large QDs, but further theoretical support would be required to make definitive conclusions. Although full quenching of PL in coupled films of larger QDs indicates no barrier to charge separation locally, it does not prohibit thermally activated transport as observed in conductivity measurements because electrical signals are likely to have contributions arising from long-range disorder.

Ligand Effects. The expected trend in T_Q from the perspective of ligand length is MPA > EDT > FA, which is faithfully upheld based upon the low temperature shift of PL from QD films treated with these ligands (Figure 2). However, the experimentally observed trend in T_Q is FA > MPA > EDT, which suggests that the functional group of the ligand plays an active role in determining the activation energy of charge separation and PL quenching. Thiols bind strongly to the QD surface (they readily replace longer chain carboxylic acids) and may passivate the excess Pb known to exist on the surface of PbS.[15] From that perspective, EDT with two thiol groups may leave the fewest electron traps and the sparsest band tail. The MPA thiol group may bind once and the carboxylate once, which, depending on the binding geometry, could lead to overall poorer passivation of the excess Pb, pushing the band tail slightly deeper. Recent studies of FA treated PbS QD films suggest that binding to the surface is stronger than that of EDT, producing a large free hole population that engenders strongly p-type films.[50] This would be consistent with our observation that prior to the strong thermal quenching via charge separation, $I_{PL}(T)$ from 13K to 80K for FA-treated films has a strong positive slope (Figure 4A), indicative of thermal escape of shallowly trapped holes from dark states.[16] If FA binding is indeed stronger than EDT, it may be that the decreased PL due to thermal release of carriers from the band tail in FA treated films is offset by the trend of increased PL with T due to release of holes from dark trap states, causing T_Q to effectively increase. The spectral shape of PL from FA treated films is more complicated than with the other treatments, suggesting a more complex distribution of trap states. It should be noted that the QDs studied here are much smaller than those investigated in ref 50, and the surface chemistry may also be quite different.

The trend observed with increasing chain length but the same functional group is consistent with

thermal activation of carriers in sub band gap states to a transport edge that depends on interdot spacing. T_Q and T_{min} both increase with increasing chain length from EDT to PDT to BDT, suggesting inhibited access to transport levels for carriers in the band tail. This is depicted in the far right feature in Figure 7B, where the overall DOS/cm^3 has decreased with BDT vs. EDT treatment. This increased distance between QDs decreases the charge separation rate and pushes the transport edge (the energy at which the rate of charge separation is faster than emission or retrapping in the band tail) significantly higher, away from the bottom of the band tail and toward the edge of the core state distribution. The larger separation between the transport edge and the bottom of the band tail essentially defines T_Q and $1/\beta$ and thus causes their increase with longer ligands.

Interestingly, the rise in T_Q and T_{min} is much larger going from PDT to BDT than from EDT to PDT despite the addition of the same length of ligand chain (Figure 6). Similar behavior was also observed in the electron (but not the hole) mobility of PbSe films,[12] in which electron mobility dropped modestly from EDT to PDT and then abruptly from PDT to BDT. It has been shown that EDT and PDT can bind in a bidentate fashion to Ag surfaces in a "*gauche*−*gauche*" rotamer,[51,52] while such a conformation of BDT would probably not lead to bidentate binding of both thiol groups to the same QD. The reduced interparticle spacing from what is predicted for *gauche*−*trans* or *trans*−*trans* conformers in EDT and PDT (but not in BDT) could be responsible for the larger than expected change in T_Q and mobility.

Connections to Transport. Passivating deep trap states is certainly helpful for improving transport, but having a considerable number (i.e., exceeding the percolation threshold) of shallow trap states may not be terribly detrimental for photocurrent, leading to moderate mobilities and high short-circuit currents. With tightly coupled QDs and thus highly interacting QD surfaces, such states may overlap and provide a relatively smooth energy landscape for carriers to navigate, without inducing excessive recombination. However, achieving true band-like transport and the associated benefits for device performance may require the elimination of nearly all surface states and fabrication of QD films with long-range order.

Similar, and even slightly narrower, band tail widths observed here in QDs compared with disordered bulk samples suggest that despite more interfaces and a large size distribution, colloidal methods produce few bulk lattice defects or impurities and maintain uniform surfaces that have comparable or smaller effective energetic disorder compared with their counterparts grown using other methods. The trend of β with chemical treatment suggests that specific ligand species could be matched with a particular QD size and material for tuning the band tail depth.

CONCLUSIONS

Thermally activated PL quenching data presented here on PbS QD films has provided insight into the nature of charge trapping and short-range transport following photoexcitation. Ligand length and functional group dependence, the lack of size distribution dependence, and the strong low temperature PL quenching for large QDs support a model of a tailing density of sub band gap states. The band tail is surprisingly narrow and trends to a minimum as the QD size gets larger due to either changing surface chemistry or a size-independent distribution of trap energies that exceeds the band edge for large sizes. This narrowing likely reduces the time carriers spend in deeper trap states and may explain the observed rise in electron mobility with increasing QD size. Further work on photoconductivity and impedance measurements will be required to elucidate the exact role that this band tail may play in transport in photovoltaic or optoelectronic device architectures.

MATERIALS AND METHODS

QD Synthesis. PbS QDs were synthesized with a first exciton peak spanning from 750 to 1650 nm (2.3 to 7.0 nm diameter) by adding 0.47 g PbO, 2−20 g oleic acid depending on desired QD size, and 10 g 1-octadecene to a three-neck round-bottom flask. This mixture was heated to 120 °C under vacuum and then kept under N_2. In a glovebox, 210 μL hexamethyldisilathiane was mixed with 4 mL 1-octadecene and loaded into a syringe. The contents of the syringe were injected into the flask and with the heating mantle removed the QDs cooled to room temperature over 20 min. The smallest QDs required lower injection temperature and less sulfur precursor. The reaction solution was mixed with 8 mL hexane and 20 mL ethanol and centrifuged to extract the QDs. Hexane and ethanol were used for an additional purification step, and the QDs were then suspended in hexane with oleate molecules capping the QDs and stored in a nitrogen glovebox. Formic acid (FA), 3-mercaptopropionic acid (MPA), 1,2-ethanedithiol (EDT), acid (OA), 1,3-propanedithiol (PDT), 1,4-butanedithiol (BDT), oleic acid, and 1-octadecene were obtained from Aldrich and used without further purification.

The PbS QD layers were deposited in a layer-by-layer fashion as described previously.[1,2] Briefly, PbS QD films were deposited by 10−30 iterations of sequentially immersing the substrate into PbS QDs in hexane (concentration 10 mg/mL) and then either 1 mM EDT, 10 mM MPA, 10 mM FA, 10 mM PDT or 10 mM BDT depending on ligand treatment.

All sample preparation was conducted in an inert atmosphere to prevent unwanted oxygen exposure, and samples were transported for measurements in a sealed capsule. Films were sandwiched between two sapphire substrates, spaced by an O-ring, and tightly screwed into a copper tube with a retaining ring. While this capsule proved inadequate to prevent oxygen exposure over a period of days, it was more than sufficient to protect samples for the approximately 10-min period required to transport them from an inert-atmosphere glovebox and load them into the optical measurement chamber.

Spectroscopic Measurements. Room-temperature absorption spectra, measured for the purpose of determining QD diameter, were recorded on a Shimadzu UV-3600 spectrophotometer. These measurements were made using the sealed capsules described above, and took <5 min to record under low-intensity light; the threat of oxidation or photo-oxidation was minimal. Temperature-dependent absorption spectra were conducted under vacuum ($<10^{-5}$ Torr) in a closed-loop He cryostat. A 100 W tungsten filament lamp, chopped at 300 Hz, was used as a source for low temperature absorption measurements. Films were excited with 15−40 mW Ar-ion laser excitation at 488 nm. The excitation beam was unfocused (spot size roughly 3 mm diameter) and mechanically chopped at 1 kHz. The resulting PL spectra were detected with an amplified Si, Ge, or InSb photodiode (varying with the needed wavelength range) routed to a lock-in amplifier. Spectra were corrected for monochromator and detector efficiencies using a calibrated lamp. For each sample, absorption and PL spectra were measured at a range of temperatures between 13 and 325 K, at intervals of 10−30 K; spectra were always collected beginning at the lowest temperature and warming up to the highest. Samples were left stationary in the cryostat during measurement of an entire temperature range. No rapid photobleaching or degradation effects were observed during PL measurements. At powers <50 mW, successive, repeated measurements at the same temperature produced identical emission spectra.

Conflict of Interest: The authors declare no competing financial interest.

Acknowledgment. We thank Arthur Nozik and Matt Law for insightful comments. This work was performed in the Center for Advanced Solar Photophysics (CASP), an Energy Frontier Research Center funded by the U.S. Department of Energy, Office of Science, Office of Basic Energy Sciences. DOE funding was provided to the National Renewable Energy Laboratory (NREL) through contract DE-AC36-08GO28308.

Supporting Information Available: Supporting Information contains absorption spectra vs. temperature, complete PL spectra vs. temperature for all samples, and excitation power dependence. This material is available free of charge via the Internet at http://pubs.acs.org.

REFERENCES AND NOTES

1. Luther, J. M.; Law, M.; Beard, M. C.; Song, Q.; Reese, M. O.; Ellingson, R. J.; Nozik, A. J. Schottky Solar Cells Based on Colloidal Nanocrystal Films. *Nano Lett.* **2008**, *8*, 3488–3492.
2. Gao, J. B.; Perkins, C. L.; Luther, J. M.; Hanna, M. C.; Chen, H. Y.; Semonin, O. E.; Nozik, A. J.; Ellingson, R. J.; Beard, M. C. n-Type Transition Metal Oxide as a Hole Extraction Layer in PbS Quantum Dot Solar Cells. *Nano Lett.* **2011**, *11*, 3263–3266.
3. Tang, J.; Kemp, K. W.; Hoogland, S.; Jeong, K. S.; Liu, H.; Levina, L.; Furukawa, M.; Wang, X.; Debnath, R.; Cha, D.; *et al.* Colloidal-Quantum-Dot Photovoltaics Using Atomic-Ligand Passivation. *Nat. Mater.* **2011**, *10*, 765–771.
4. Nozik, A. J.; Beard, M. C.; Luther, J. M.; Law, M.; Ellingson, R. J.; Johnson, J. C. Semiconductor Quantum Dots and Quantum Dot Arrays and Applications of Multiple Exciton Generation to Third-Generation Photovoltaic Solar Cells. *Chem. Rev.* **2010**, *110*, 6873–6890.
5. Luther, J. M.; Gao, J. B.; Lloyd, M. T.; Semonin, O. E.; Beard, M. C.; Nozik, A. J. Stability Assessment on a 3% Bilayer PbS/ZnO Quantum Dot Heterojunction Solar Cell. *Adv. Mater.* **2010**, *22*, 3704–3707.
6. Talapin, D. V.; Lee, J. S.; Kovalenko, M. V.; Shevchenko, E. V. Prospects of Colloidal Nanocrystals for Electronic and Optoelectronic Applications. *Chem. Rev.* **2010**, *110*, 389–458.
7. Kang, M. S.; Sahu, A.; Norris, D. J.; Frisbie, C. D. Size- and Temperature-Dependent Charge Transport in PbSe Nanocrystal Thin Films. *Nano Lett.* **2011**, *11*, 3887–3892.
8. Mentzel, T. S.; Porter, V. J.; Geyer, S.; MacLean, K.; Bawendi, M. G.; Kastner, M. A. Charge Transport in PbSe Nanocrystal Arrays. *Phys. Rev. B* **2008**, *77*, 075316.
9. Talgorn, E.; Gao, Y. N.; Aerts, M.; Kunneman, L. T.; Schins, J. M.; Savenije, T. J.; van Huis, M. A.; van der Zant, H. S. J.; Houtepen, A. J.; Siebbeles, L. D. A. Unity Quantum Yield of Photogenerated Charges and Band-like Transport in Quantum-Dot Solids. *Nat. Nanotech.* **2011**, *6*, 733–739.
10. Nagpal, P.; Klimov, V. I. Role of Mid-gap States in Charge Transport and Photoconductivity in Semiconductor Nanocrystal Films. *Nat. Commun.* **2011**, *2*, 486.
11. Tang, J. A.; Sargent, E. H. Infrared Colloidal Quantum Dots for Photovoltaics: Fundamentals and Recent Progress. *Adv. Mater.* **2011**, *23*, 12–29.
12. Liu, Y.; Gibbs, M.; Puthussery, J.; Gaik, S.; Ihly, R.; Hillhouse, H. W.; Law, M. Dependence of Carrier Mobility on Nanocrystal Size and Ligand Length in PbSe Nanocrystal Solids. *Nano Lett.* **2010**, *10*, 1960–1969.
13. Allan, G.; Delerue, C. Confinement Effects in PbSe Quantum Wells and Nanocrystals. *Phys. Rev. B* **2004**, *70*, 245321.
14. Franceschetti, A. Structural and Electronic Properties of PbSe Nanocrystals from First Principles. *Phys. Rev. B* **2008**, *78*, 075418.
15. Moreels, I.; Fritzinger, B.; Martins, J. C.; Hens, Z. Surface Chemistry of Colloidal PbSe Nanocrystals. *J. Am. Chem. Soc.* **2008**, *130*, 15081–15086.
16. Hughes, B. K.; Ruddy, D.; Nozik, A. J.; Johnson, C. J.; Beard, M. C. Control of PbSe Quantum Dot Surface Chemistry and Photophysics Using an Alkylselenide Ligand. *ACS Nano* **2012**, submitted.
17. Chappell, H. E.; Hughes, B. K.; Beard, M. C.; Nozik, A. J.; Johnson, J. C. Emission Quenching in PbSe Quantum Dot Arrays by Short-Term Air Exposure. *J. Phys. Chem. Lett.* **2011**, *2*, 889–893.
18. Fernee, M. J.; Thomsen, E.; Jensen, P.; Rubinsztein-Dunlop, H. Highly Efficient Luminescence from a Hybrid State Found in Strongly Quantum Confined PbS Nanocrystals. *Nanotechnology* **2006**, *17*, 956–962.
19. Lewis, J. E.; Wu, S.; Jiang, X. J. Unconventional Gap State of Trapped Exciton in Lead Sulfide Quantum Dots. *Nanotechnology* **2010**, *21*, 455402.
20. Park, S. H.; Cho, Y. H. Strain and Piezoelectric Potential Effects on Optical Properties in CdSe/CdS Core/Shell Quantum Dots. *J. Appl. Phys.* **2011**, *109*, 113103.
21. Chen, Y.; Vela, J.; Htoon, H.; Casson, J. L.; Werder, D. J.; Bussian, D. A.; Klimov, V. I.; Hollingsworth, J. A. "Giant" Multishell CdSe Nanocrystal Quantum Dots with Suppressed Blinking. *J. Am. Chem. Soc.* **2008**, *130*, 5026–5027.
22. Murphy, J. E.; Beard, M. C.; Nozik, A. J. Time-resolved Photoconductivity of PbSe Sanocrystal Arrays. *J. Phys. Chem. B* **2006**, *110*, 25455–25461.
23. Piris, J.; Ferguson, A. J.; Blackburn, J. L.; Norman, A. G.; Rumbles, G.; Selmarten, D. C.; Kopidakis, N. Efficient Photoinduced Charge Injection from Chemical Bath Deposited CdS into Mesoporous TiO_2 Probed with Time-resolved Microwave Conductivity. *J. Phys. Chem. C* **2008**, *112*, 7742–7749.
24. Street, R. A. Luminescence and Recombination in Hydrogenated Amorphous-Silicon. *Adv. Phys.* **1981**, *30*, 593–676.
25. Tsang, C.; Street, R. A. Recombination in Plasma-Deposited Amorphous Si-H - Luminescence Decay. *Phys. Rev. B* **1979**, *19*, 3027–3040.
26. Werner, J.; Peisl, M. Exponential Band Tails in Polycrystalline Semiconductor-Films. *Phys. Rev. B* **1985**, *31*, 6881–6883.
27. Cody, G. D.; Tiedje, T.; Abeles, B.; Brooks, B.; Goldstein, Y. Disorder and the Optical-Absorption Edge of Hydrogenated Amorphous-Silicon. *Phys. Rev. Lett.* **1981**, *47*, 1480–1483.
28. Pejova, B.; Abay, B.; Bineva, I. Temperature Dependence of the Band-Gap Energy and Sub-Band-Gap Absorption Tails in Strongly Quantized ZnSe Nanocrystals Deposited as Thin Films. *J. Phys. Chem. C* **2010**, *114*, 15280–15291.
29. Hanna, M. C.; Nozik, A. J. Solar Conversion Efficiency of Photovoltaic and Photoelectrolysis Cells with Carrier Multiplication Absorbers. *J. Appl. Phys.* **2006**, *100*, 074510.
30. Miller, O. D.; Yablanovitch, E.; Kurtz, S. R. Intense Internal and External Fluorescence as Solar Cells Approach the

Shockley-Queisser Efficiency Limit. http://arxiv.org/abs/1106.1603, 2012.
31. Moreels, I.; Lambert, K.; Smeets, D.; De Muynck, D.; Nollet, T.; Martins, J. C.; Vanhaecke, F.; Vantomme, A.; Delerue, C.; Allan, G.; Hens, Z. Size-Dependent Optical Properties of Colloidal PbS Quantum Dots. *ACS Nano* **2009**, *3*, 3023–3030.
32. Law, M.; Luther, J. M.; Song, O.; Hughes, B. K.; Perkins, C. L.; Nozik, A. J. Structural, Optical, and Electrical Properties of PbSe Nanocrystal Solids Treated Tthermally or with Simple Amines. *J. Am. Chem. Soc.* **2008**, *130*, 5974–5985.
33. Olkhovets, A.; Hsu, R. C.; Lipovskii, A.; Wise, F. W. Size-Dependent Temperature Variation of the Energy Gap in Lead-Salt Quantum Dots. *Phys. Rev. Lett.* **1998**, *81*, 3539–3542.
34. Kigel, A.; Brumer, M.; Maikov, G. I.; Sashchiuk, A.; Lifshitz, E. Thermally Activated Photoluminescence in Lead Selenide Colloidal Quantum Dots. *Small* **2009**, *5*, 1675–1681.
35. Odonnell, K. P.; Chen, X. Temperature-Dependence of Semiconductor Band-Gaps. *Appl . Phys. Lett.* **1991**, *58*, 2924–2926.
36. Gaponenko, M. S.; Lutich, A. A.; Tolstik, N. A.; Onushchenko, A. A.; Malyarevich, A. M.; Petrov, E. P.; Yumashev, K. V. Temperature-Dependent Photoluminescence of PbS Quantum Dots in Glass: Evidence of Exciton State Splitting and Carrier Trapping. *Phys. Rev. B* **2010**, *82*, 125320.
37. Schaller, R. D.; Crooker, S. A.; Bussian, D. A.; Pietryga, J. M.; Joo, J.; Klimov, V. I. Revealing the Exciton Fine Structure of PbSe Nanocrystal Quantum Dots Using Optical Spectroscopy in High Magnetic Fields. *Phys. Rev. Lett.* **2010**, *105*, 067403.
38. Lee, J. S.; Kovalenko, M. V.; Huang, J.; Chung, D. S.; Talapin, D. V. Band-like Transport, High Electron Mobility and High Photoconductivity in All-Inorganic Nanocrystal Arrays. *Nat. Nanotech.* **2011**, *6*, 348–352.
39. Semonin, O. E.; Johnson, J. C.; Luther, J. M.; Midgett, A. G.; Nozik, A. J.; Beard, M. C. Absolute Photoluminescence Quantum Yields of IR-26 Dye, PbS, and PbSe Quantum Dots. *J. Phys. Chem. Lett.* **2010**, *1*, 2445–2450.
40. Poles, E.; Selmarten, D. C.; Micic, O. I.; Nozik, A. J. Anti-Stokes Photoluminescence in Colloidal Semiconductor Quantum Dots. *Appl. Phys. Lett.* **1999**, *75*, 971–973.
41. Zhang, L. Y.; Yin, L. W.; Wang, C. X.; Lun, N.; Qi, Y. X.; Xiang, D. Origin of Visible Photoluminescence of ZnO Quantum Dots: Defect-Dependent and Size-Dependent. *J. Phys. Chem. C* **2010**, *114*, 9651–9658.
42. Nirmal, M.; Norris, D. J.; Kuno, M.; Bawendi, M. G.; Efros, A. L.; Rosen, M. Observation of the Dark Exciton in Cdse Quantum Dots. *Phys. Rev. Lett.* **1995**, *75*, 3728–3731.
43. An, J. M.; Franceschetti, A.; Zunger, A. The Excitonic Exchange Splitting and Radiative Lifetime in PbSe Quantum Dots. *Nano Lett.* **2007**, *7*, 2129–2135.
44. Lu, W.; Kamiya, I.; Ichida, M.; Ando, H. Temperature Dependence of Electronic Energy Transfer in PbS Quantum Dot Films. *Appl. Phys. Lett.* **2009**, *95*, 083102.
45. Wuister, S. F.; Koole, R.; Donega, C. D.; Meijerink, A. Temperature-Dependent Energy Transfer in Cadmium Telluride Quantum Dot Solids. *J. Phys. Chem. B* **2005**, *109*, 5504–5508.
46. Choi, J. J.; Luria, J.; Hyun, B. R.; Bartnik, A. C.; Sun, L. F.; Lim, Y. F.; Marohn, J. A.; Wise, F. W.; Hanrath, T. Photogenerated Exciton Dissociation in Highly Coupled Lead Salt Nanocrystal Assemblies. *Nano Lett.* **2010**, *10*, 1805–1811.
47. Kang, I.; Wise, F. W. Electronic Structure and Optical Properties of PbS and PbSe Quantum Dots. *J. Opt. Soc. Am. B* **1997**, *14*, 1632–1646.
48. Savchouk, A. U.; Ostapenko, S.; Nowak, G.; Lagowski, J.; Jastrzebski, L. Band-Tail Photoluminescence in Polycrystalline Silicon Thin-Films. *Appl. Phys. Lett.* **1995**, *67*, 82–84.
49. Boulitrop, F.; Dunstan, D. J. Phonon Interactions in the Tail States of Alpha-Si-H. *Phys. Rev. B* **1983**, *28*, 5923–5929.
50. Zarghami, M. H.; Liu, Y.; Gibbs, M.; Gebremichael, E.; Webster, C.; Law, M. p-Type PbSe and PbS Quantum Dot Solids Prepared with Short-Chain Acids and Diacids. *ACS Nano* **2010**, *4*, 2475–2485.
51. Joo, S. W.; Han, S. W.; Kim, K. Adsorption Characteristics of 1,3-Propanedithiol on Gold: Surface-Enhanced Raman Scattering and Ellipsometry Study. *J. Phys. Chem. B* **2000**, *104*, 6218–6224.
52. Joo, S. W.; Han, S. W.; Kim, K. Multilayer Formation of 1,2-Ethanedithiol on Gold: Surface-Enhanced Raman Scattering and Ellipsometry Study. *Langmuir* **2000**, *16*, 5391–5396.